

Does diffusion kurtosis imaging lead to better neural tissue characterization? A rodent brain maturation study

Matthew M. Cheung^{a,b}, Edward S. Hui^{a,b}, Kevin C. Chan^{a,b}, Joseph A. Helpert^c, Liqun Qi^d, Ed X. Wu^{a,b,*}

^a Laboratory of Biomedical Imaging and Signal Processing, The University of Hong Kong, Pokfulam, Hong Kong, People's Republic of China

^b Department of Electrical and Electronic Engineering, The University of Hong Kong, Pokfulam, Hong Kong, People's Republic of China

^c Department of Radiology, New York University School of Medicine, New York, New York, USA

^d Department of Applied Mathematics, The Hong Kong Polytechnic University, Hung Hom, Hong Kong, People's Republic of China

ARTICLE INFO

Article history:

Received 2 August 2008

Revised 28 October 2008

Accepted 8 December 2008

Available online 25 December 2008

Keywords:

MRI

Directional kurtosis

Diffusion kurtosis tensor

DKI

Developing brain

ABSTRACT

Diffusion kurtosis imaging (DKI) can be used to estimate excess kurtosis, which is a dimensionless measure for the deviation of water diffusion profile from Gaussian distribution. Several recent studies have applied DKI to probe the restricted water diffusion in biological tissues. The directional analysis has also been developed to obtain the directionally specific kurtosis. However, these studies could not directly evaluate the sensitivity of DKI in detecting subtle neural tissue alterations. Brain maturation is known to involve various biological events that can affect water diffusion properties, thus providing a sensitive platform to evaluate the efficacy of DKI. In this study, *in vivo* DKI experiments were performed in normal Sprague–Dawley rats of 3 different ages: postnatal days 13, 31 and 120 ($N=6$ for each group). Regional analysis was then performed for 4 white matter (WM) and 3 gray matter (GM) structures. Diffusivity and kurtosis estimates derived from DKI were shown to be highly sensitive to the developmental changes in these chosen structures. Conventional diffusion tensor imaging (DTI) parameters were also computed using monoexponential model, yielding reduced sensitivity and directional specificity in monitoring the brain maturation changes. These results demonstrated that, by measuring directionally specific diffusivity and kurtosis, DKI offers a more comprehensive and sensitive detection of tissue microstructural changes. Such imaging advance can provide a better MR diffusion characterization of neural tissues, both WM and GM, in normal, developmental and pathological states.

© 2008 Elsevier Inc. All rights reserved.

Introduction

Magnetic resonance (MR) diffusion tensor imaging (DTI) has been shown to provide unique structural information in characterizing tissue microstructure (Basser, 1995; Basser and Pierpaoli, 1996), which cannot be easily revealed non-invasively by other modalities. The three-dimensional water diffusion probability distribution in an anisotropic medium has been quantified by a rank 2 tensor in DTI (Basser, 1995) where the three eigenvectors correspond to the axes of a tri-axial diffusivity ellipsoid. The commonly employed rotationally invariant parameters derived from the diffusion tensor (DT) include the mean diffusivity (MD), fractional anisotropy (FA), axial diffusivity (λ_{\parallel}) and radial diffusivity (λ_{\perp}). It has been observed that water diffusion is anisotropic in the central nervous system (Moseley et al., 1990). The origin of the anisotropy in white matter (WM) nerve fibers can be complex and it cannot be solely ascribed to myelination (Beaulieu, 2002). Inherent structures of axons can also alter the diffusion properties. The degree of anisotropy and the directional

diffusivities have been shown to correlate well with microstructural changes of neural tissues in certain pathological states (Beaulieu et al., 1996; Song et al., 2003; Sun et al., 2006).

The orientational neuroarchitecture can be inferred from DTI, but it is inadequate to resolve the heterogeneity within a voxel (Tuch et al., 2002). For instance, crossing or diverging WM fibers can appear to be isotropic and DTI may fail to sensitively probe these structures. Moreover, the gray matter (GM) is relatively isotropic and DTI is not truly effective in characterizing water diffusion changes in GM. Apart from the inability to resolve the heterogeneity, the assumption of monoexponential signal attenuation in DTI due to diffusion was observed to be invalid when a high b -value was employed (Assaf and Cohen, 1998; Basser and Jones, 2002; Mulkern et al., 1999; Niendorf et al., 1996). DTI estimation of diffusivity is based on the implicit assumption that diffusion occurs in an unrestricted environment. In biological tissues, there is always structural hindrance or restriction that prohibits truly free water diffusion and hence we can apply a higher b -value to probe such restricted diffusion. The deviation from the monoexponential decay leads to the fact that the apparent diffusion coefficient depends on the b -values chosen, complicating quantitative and comparative studies. There are various approaches to characterize or quantify this non-monoexponential decay. As there

* Corresponding author. Fax: +852 2559 8738.
E-mail address: ewu@eee.hku.hk (E.X. Wu).

are at least two types of compartments (intra- and extra-cellular) in the tissue, a bi-exponential model was proposed (Mulkern et al., 1999; Niendorf et al., 1996). Despite the good fit of the signal attenuation, the estimated volume fractions of the fast and slow diffusion components were found to be inconsistent with the known ratio between the intra-cellular and extra-cellular compartments (Clark et al., 2002; Clark and Le Bihan, 2000; Minati et al., 2007; Niendorf et al., 1996).

More generalized approaches have been attempted. Q-space imaging estimates the water diffusion displacement probability profile (Callaghan, 1991) and it has been shown that structural changes in diseased neural tissues can be detected. (Assaf et al., 2003, 2005; Biton et al., 2006; Nossin-Manor et al., 2007). Although q-space can fully describe the diffusion profile, it often requires prohibitively long scan time and is hardware demanding. The Bloch–Torrey equation for diffusion has been generalized for a multiple rank tensor in generalized DTI (GDTI) (Liu et al., 2004; Ozarslan and Mareci, 2003). Formulations have been introduced, but they have not shown much success in practice because the approach lacks physical relevance and interpretation is problematic. Diffusion kurtosis imaging (DKI) has been proposed recently to probe non-Gaussian diffusion property (Jensen and Helpert, 2003; Jensen et al., 2005; Lu et al., 2006). DKI provides a second-order approximation of water displacement distribution, in which both the apparent diffusion coefficient and apparent diffusion kurtosis can be obtained. Kurtosis here refers to the excess kurtosis and is the normalized and standardized fourth central moment of water displacement distribution (Jensen et al., 2005). It is a dimensionless measure quantifying the deviation of the water diffusion profile from Gaussian distribution (that is inherent to free or unrestricted diffusion), and hence revealing the degree of diffusion restriction. A positive kurtosis implies that the distribution is more sharply peaked than a Gaussian one. Both diffusivity and kurtosis are fitted from a non-monoexponential equation in DKI. The diffusivity estimated is different from that computed using the monoexponential model unless the kurtosis is zero. Although in theory DKI is robust, the sensitivity of this approach for tissue characterization has not yet been evaluated.

There were a few human brain studies that measured mean kurtosis (MK) to detect pathological changes in neural tissues (Falangola et al., 2007a,b; Helpert et al., 2007; Jensen et al., 2005; Latt et al., 2008; Lu et al., 2006; Minati et al., 2007; Ramani et al., 2007). They demonstrated that MK can yield information different from the FA obtained with DTI and that MK can detect pathophysiological changes. In recent studies, directional kurtosis analysis was formulated and applied to examine the effect of rat brain fixation (Hui et al., 2008; Qi et al., 2008). Directional kurtoses along the eigenvectors of DT were computed by orthogonal transformation (Hui et al., 2008; Qi et al., 2008), providing directionally specific kurtosis information. The study demonstrated that various kurtosis estimates can reveal information different from diffusivity estimates, and the effect of fixation was documented. Due to the dramatic structural changes involved in fixation, the study cannot directly evaluate how sensitive DKI can detect neural tissue alterations. In the current study, *in vivo* rat brain maturation was studied by DKI to investigate the efficacy of DKI in detecting subtle morphological changes in neural tissues.

There are various biological events that can affect water diffusion properties in both WM and GM during normal brain maturation. DTI has been applied in various human (Dubois et al., 2006; Huang et al., 2006; Huppi and Dubois, 2006; Neil et al., 2002; Suzuki et al., 2003) and rodent studies (Bockhorst et al., 2008; Chahboune et al., 2007; Harsan et al., 2006; Larvaron et al., 2007; Mori et al., 2001; Sizonenko et al., 2007; Verma et al., 2005; Zhang et al., 2003) and it was found to be sensitive to brain development. WM maturation processes include denser packing of fiber bundles and axons, increased axon diameter and number of neurofibrils, and changes

of axonal membrane permeability (Dubois et al., 2006; Huppi and Dubois, 2006; Larvaron et al., 2007; Neil et al., 2002; Suzuki et al., 2003). There is also increased complexity in extracellular matrix and microtubule associated proteins (Huppi and Dubois, 2006; Neil et al., 2002; Suzuki et al., 2003). In GM, apart from the addition of basal dendrites, modification in tissue water content and cell packing density, it is known that changes in cortical cytoarchitecture affect the water diffusion behavior (Bockhorst et al., 2008; Huppi and Dubois, 2006; Sizonenko et al., 2007). The anisotropic diffusion observed in immature cortex is believed to be caused by radial glial cells. The transition of radial glia to astrocytic neuropil is shown to reduce the anisotropy when the brain matures (Bockhorst et al., 2008; Sizonenko et al., 2007). These subtle developmental changes in normal rat brain maturation can provide an effective biological platform to evaluate the sensitivity of DKI. Furthermore, hypoxic-ischemic insults in neonates cause mild but persistent injuries in both WM and GM (Wang et al., 2008; Wang et al., 2006; Yang et al., 2008; Yang and Wu, 2008). To study these pathological changes in neonates, normal brain developmental changes have to be documented in depth (Bockhorst et al., 2008). A recent longitudinal study of normal rat brain development showed that DTI parameters were correlated with the maturation processes (Bockhorst et al., 2008). However, the use of a single non-zero *b*-value in the study might limit the interpretation of the DTI findings in view of the complex maturation processes. Most of the other rodent brain developmental studies were either performed *ex vivo* or focused on few particular structures. However, *ex vivo* studies may not truly exploit the power of MR diffusion in the study of developmental brain. Although the diffusion anisotropy was maintained after fixation (Sun et al., 2005), directional diffusivities and kurtoses can change substantially and vary with sample temperature (Hui et al., 2008). Thus their absolute values cannot be used for comparison among studies in a robust manner.

In this study, normal postnatal rat brain development was investigated to assess the sensitivity of DKI. Directional kurtosis analysis was employed so that the kurtoses along the DT eigenvectors could be measured. Various WM and GM structures were analyzed for different postnatal stages. In addition, these diffusivity and kurtosis parameters were compared with those derived from the monoexponential model used by conventional DTI.

Materials and methods

Theory

Conventional DTI assumes Gaussian (i.e., unrestricted and free) diffusion. The apparent diffusivity (D_{app}) is derived by linearly fitting the DW signals acquired with one or more non-zero *b*-values to the following linear equation:

$$\ln [S(b)/S(0)] = -bD_{app}. \quad (1)$$

In DKI, logarithmic expansion of signal decay is used to estimate both apparent diffusivity and diffusion kurtosis (K_{app}) (Jensen et al., 2005; Lu et al., 2006). Kurtosis is a quantitative measurement of the deviation from Gaussian form. DW signals are used to estimate D_{app} and K_{app} along an applied diffusion gradient direction with the following equation:

$$\ln [S(b)/S(0)] = -bD_{app} + \frac{1}{6}b^2D_{app}^2K_{app}, \quad (2)$$

where $S(b)$ is the DW signal intensity at a particular *b*-value, and $S(0)$ the signal without applying any diffusion gradient. MK is defined as the kurtosis averaged among all directions. Note that 15 independent elements are required to construct the 4th order diffusion kurtosis tensor (KT). KT can be transformed to a coordinate system formed by

the three orthogonal eigenvectors of the 2nd order DT (Hui et al., 2008; Qi et al., 2008):

$$\hat{W}_{ijkl} = \sum_{i'=1}^3 \sum_{j'=1}^3 \sum_{k'=1}^3 \sum_{l'=1}^3 e_{i'i} e_{j'j} e_{k'k} e_{l'l} W_{i'j'k'l'}, \quad (3)$$

The kurtosis along an individual DT eigenvector can be computed from the transformed KT(\hat{W}):

$$K_i = \frac{MD^2}{\lambda_i^2} \cdot \hat{W}_{iiii}, \quad (4)$$

where λ_i are the eigenvalues of the DT ($\lambda_1 > \lambda_2 > \lambda_3$). Axial kurtosis ($K_{//}$) and radial kurtosis (K_{\perp}) can then be derived (Hui et al., 2008; Qi et al., 2008).

$$K_{//} = K_1 \quad (5)$$

is the kurtosis along the principal eigenvector of DT, and

$$K_{\perp} = \frac{K_2 + K_3}{2} \quad (6)$$

is the average kurtosis along the other two eigenvectors.

Animal preparation

All animal experiments were approved by the local animal research ethics committee. Experiments were conducted in three separate groups of normal Sprague–Dawley rats of different ages: postnatal day 13 (31–38 g), 31 (86–110 g) and 120 (250–300 g). The litters were culled to 9 to 13 pups and bred in regular light/dark cycle. Sample size was 6 for each age group. After MRI, animals were euthanized.

Data acquisition

The animals were anesthetized with a mixture of isoflourane/air at 3% for induction and 1.5% for maintenance throughout the MR

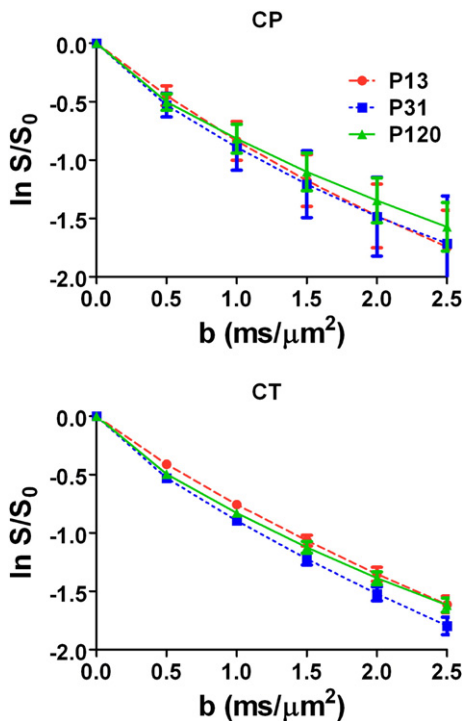


Fig. 1. Normalized signal decay curves of cerebral peduncle (CP) and cerebral cortex (CT). ROI was defined on a single slice from one animal from each age group. Signal [$\ln(S/S_0)$] is the average of all normalized DW signals along 30 gradient encoding directions. The error bar indicates the SD.

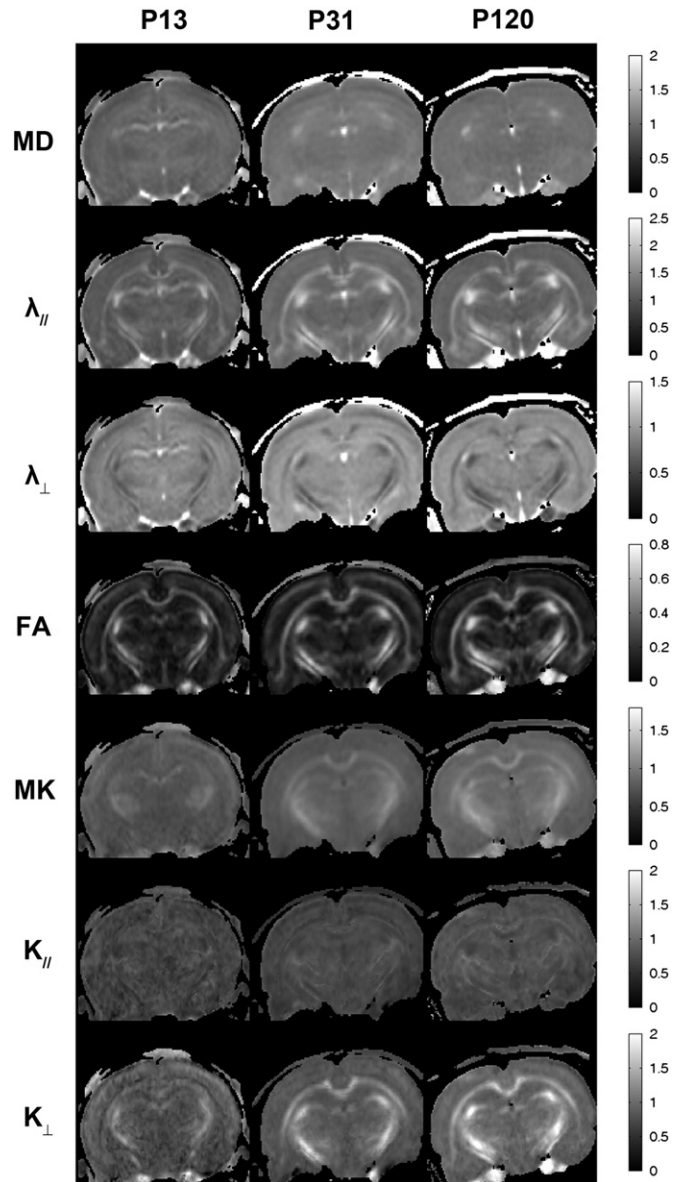


Fig. 2. Typical *in vivo* DKI-derived mean diffusivity (MD in $\mu\text{m}^2/\text{ms}$), axial diffusivity ($\lambda_{//}$ in $\mu\text{m}^2/\text{ms}$), radial diffusivity (λ_{\perp} in $\mu\text{m}^2/\text{ms}$), fractional anisotropy (FA), mean kurtosis (MK), axial kurtosis ($K_{//}$), and radial kurtosis (K_{\perp}) maps in postnatal day 13 (P13), day 31 (P31) and day 120 (P120) rat brains.

experiment. A warming pad with circulating water was used throughout the MR acquisitions. Experiments were performed on a 7 Tesla scanner with a maximum gradient of 360 mT/m (70/16 PharmaScan, Bruker Biospin GmbH, Germany). All DW images, together with five images without diffusion sensitization, were acquired with a respiration-gated spin-echo 4 shots EPI sequence with navigation echo. DW images were collected with an encoding scheme along 30 gradient encoding directions (Jones et al., 1999). The sequence was repeated four times for signal averaging, resulting in a total acquisition time of approximately 2 h depending on the actual respiration rate.

For P13 neonates, a 23 mm birdcage quadrature RF coil for both transmitting and receiving was used. Five b -values (0.5, 1, 1.5, 2, 2.5 $\text{ms}/\mu\text{m}^2$) were used along each direction. The acquisition parameters were: TR/TE=3000/33.3 ms, $\delta/\Delta=5/20$ ms, slice thickness=0.7 mm (interslice gap=0.08 mm), FOV=25×25 mm^2 , data matrix=128×128, and resolution=195×195 μm^2 . For P31 and P120 rats, MR imaging was performed with a birdcage transmit-only coil with a 72 mm inner diameter in combination with an actively

decoupled receive-only quadrature surface coil. The acquisition parameters were: TR/TE=3000/30.3 ms, $\delta/\Delta=5/17$ ms, slice thickness=1 mm (interslice gap=0.1 mm), FOV=30×30 mm², data matrix=128×128, and resolution=234×234 μm^2 .

Data analysis

All DW images with varying b -values were co-registered using AIR5.2.5 (Woods et al., 1998) before they were fitted to Eq. (2) on a voxel-to-voxel basis using a Levenberg–Marquart (LM) non-linear fitting algorithm (Lu et al., 2006). Both DT and KT were computed from the fitted D_{app} and K_{app} values (Lu et al., 2006). DKI-derived kurtosis parametric maps (MK, K_{\parallel} , K_{\perp}), together with MD, FA, λ_{\parallel} and λ_{\perp} maps (Basser and Pierpaoli, 1996; Song et al., 2003), were obtained.

Regions of interest (ROIs) were manually defined in several coronal slices by referencing to the standard rat brain atlas (Paxinos and Watson, 2005). Anatomical landmarks were identified from both FA

and MK maps in each animal. As MK map is less susceptible to the partial volume effect of cerebral spinal fluid (Hu et al., 2008), ROI was delineated in MK maps together with FA maps. Four WM structures, including corpus callosum (CC), external capsule (EC), cerebral peduncle (CP) and anterior commissure (AC), and 3 GM structures, namely cerebral cortex (CT), hippocampus (HP) and caudate putamen (CPu) were defined as previously illustrated (Hui et al., 2008). Various diffusivity and kurtosis parameters were computed by volume-averaging within the multi-slice ROIs for each structure. For each parameter, analysis of variance (ANOVA) was performed to compare the measurements among different age groups, followed by Tukey's test to detect inter-group differences.

To compare the diffusivities and FA estimated in DKI above with those derived using the conventional monoexponential model, all DW signals were fitted to Eq. (1) using the LM non-linear algorithm. Note that identical ROIs were used to quantify all parameters estimated by DKI and conventional DTI.

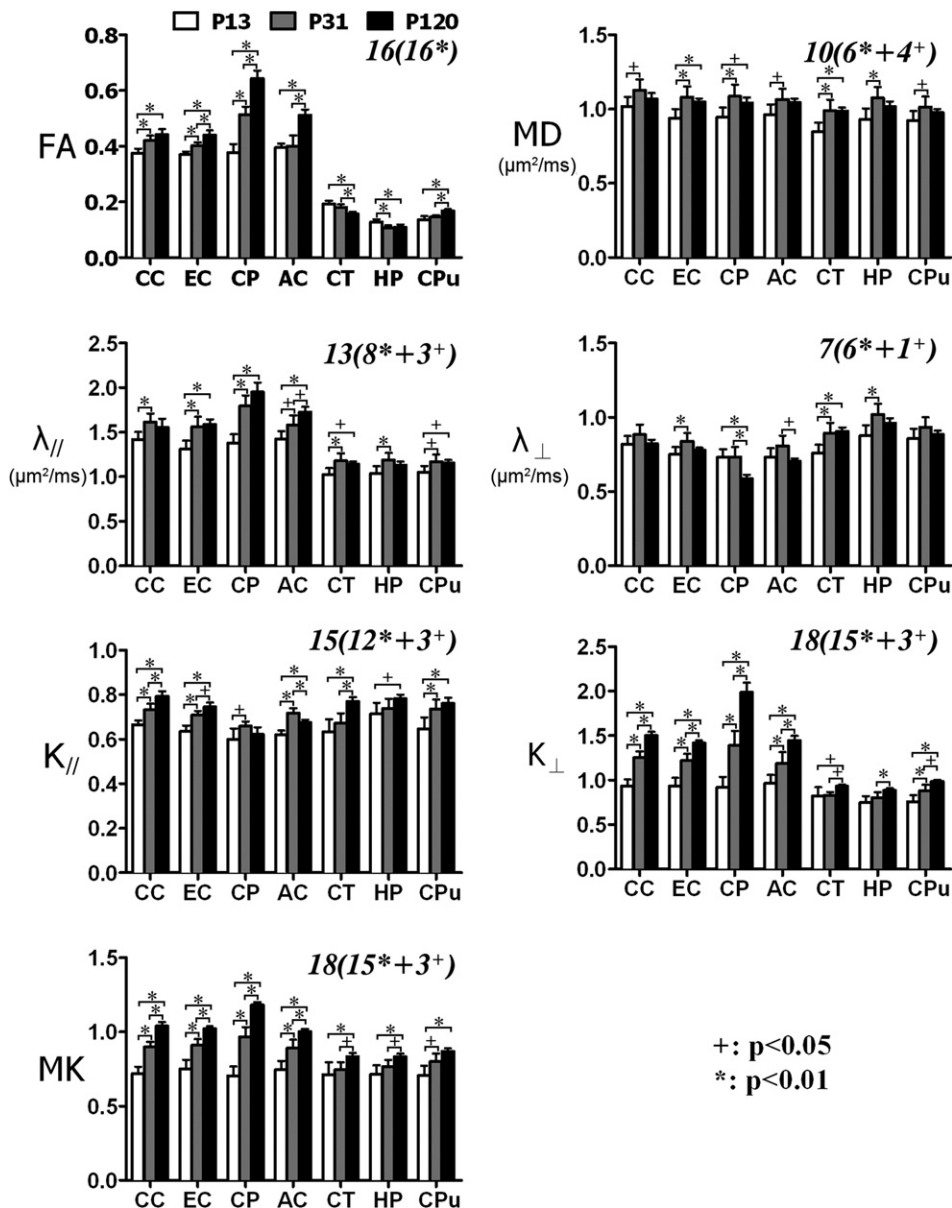


Fig. 3. DKI-derived diffusivity and kurtosis parameters for various WM and GW structures ($n=6$ per age group at postnatal days 13, 31 and 120). DW signals were fitted to the quadratic DKI model in Eq. (2) to compute all diffusivity and kurtosis parameters shown here. Error bars represent the inter-animal SDs in each age group. The statistical comparisons between 3 age groups were performed with Tukey's test after one-way ANOVA. The total number of significant changes detected by each parameter is indicated in italics.

Results

Evolution of DKI parameters with age

The representative normalized DW signal decays in CP and CT observed in the 3 age groups are shown in Fig. 1. The mean normalized signal is the average of the normalized signals along the 30 directions of diffusion encoding gradients, and the error bar indicates the standard deviation (SD). It can be clearly observed that the attenuation was not monoexponential and hence conventional DTI with a single non-zero b -value was not adequate to fully characterize the signal decay. The deviation from linearity was obvious in CP, which was more pronounced in older age groups. DW signal decay in CT also exhibited a progressive deviation, although it was less apparent than that in CP. Such increasing deviation from monoexponential b -value dependence with age indicated that the diffusion environment in GM became more restricted as brain matured. It is not surprising to observe the larger SD in WM than that in GM because of the diffusion restriction along radial direction in WM and the lack of preferential diffusion direction in GM.

Typical DKI-derived parametric maps (MD, $\lambda_{//}$, λ_{\perp} , FA, MK, $K_{//}$ and K_{\perp}) from 3 age groups are shown in Fig. 2. These parametric maps illustrate the contrast changes at different developmental stages. In particular, the contrast between WM and GM in MK and K_{\perp} increased substantially between P13 and P31. At P13, WM and GM exhibited relatively low contrasts in kurtosis maps but they could be well differentiated at P31 and P120. However, the evolution of the contrast was not obvious in the diffusivity maps.

Fig. 3 shows the various DKI-derived parameters measured for 7 structures at different developmental stages. Error bars represent the inter-animal SDs in each age group. Note that both apparent diffusivity and kurtosis along each diffusion direction were estimated by the DKI model using Eq. (2), and then employed to compute these parameters for each animal. As shown in Fig. 3, the comparisons among 3 age groups demonstrate the high sensitivity of DKI in detecting brain maturation changes. The statistical significance is

marked by an asterisk (*: $p < 0.01$) or a cross (+: $p < 0.05$). Fig. 3 shows that the combination of diffusivities and kurtoses detected all 21 developmental changes in 7 structures among 3 age groups. Mean and directional kurtoses revealed these changes in a more robust manner than their diffusivity counterparts. For example MK and K_{\perp} changes were statistically significant in 18 out of the total 21 comparisons. In general, $K_{//}$ and $\lambda_{//}$ increased moderately in both WM and GM. In WM, K_{\perp} increased substantially. Interestingly, only 7 comparisons were statistically significant in λ_{\perp} . Kurtoses have been previously shown to negatively correlate but differ from diffusivities (Hui et al., 2008). The measurements in Fig. 3 agree with this finding and demonstrated that diffusivity and kurtosis are not a simple one-to-one mapping.

Comparison between DKI and conventional DTI

Fig. 4 compares the conventional DTI parameters measured at different developmental stages. Note that apparent diffusivity along each direction was first calculated by fitting the DW signals with multiple b -values to Eq. (1). The directional diffusivities estimated in the monoexponential DTI model reflect a combined effect of the diffusivity and kurtosis derived in DKI. When there is a large kurtosis (in Fig. 3), the estimated diffusivity in conventional DTI (in Fig. 4) shows a large discrepancy with the diffusivity in DKI approach. Because the restrictive nature of tissue microstructure inhibits the free diffusion process, kurtosis in biological tissue is always positive. Therefore, DTI-derived diffusivities were generally lower than those by DKI. For example, the average MD underestimations in different WM structures at P13, P31 and P120 were 19%, 26% and 29% respectively, while those in GM structures were 19%, 22% and 24% respectively. The large discrepancies for P120 adult rats were a result of the generally higher kurtosis.

Similar to previous studies, FA detected certain developmental changes. There were 16 statistically significant comparisons using DTI-derived FA. The trend of increasing FA in WM was apparent, resulting

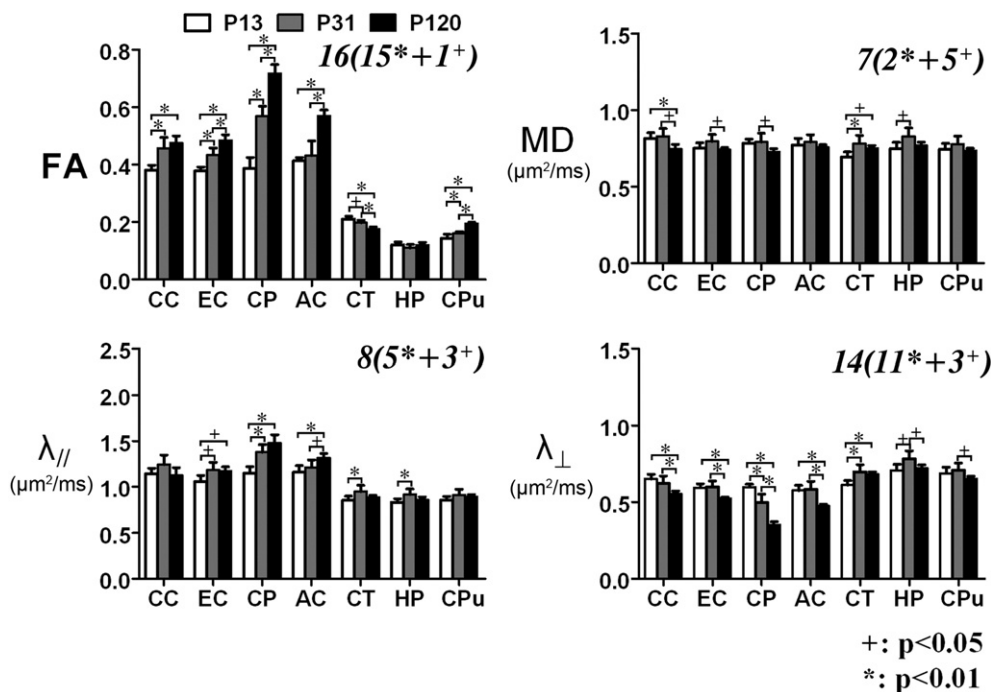


Fig. 4. Conventional DTI-derived parameters for various WM and GM structures measured using the identical ROIs in each animal. They were derived by using the conventional monoexponential model. All DW signals were fitted to Eq. (1) for the diffusivity parameters shown. Error bars represent the inter-animal SDs in each age group. The statistical comparisons between 3 age groups were performed with Tukey's test after one-way ANOVA.

from general $\lambda_{//}$ increase (except in CC) and λ_{\perp} decrease (except in EC). Although significant results in detecting developmental changes can still be obtained from conventional DTI using FA, directional diffusivities can only yield limited sensitivity when compared to directional kurtoses. For example, axial and radial diffusivities together produced 21 statistically significant detections (in Fig. 4) while their kurtosis counterparts gave 33 (in Fig. 3).

Discussions

Evolution of DKI parameters with age

In the direction along the principal eigenvector of DT, the generally increased diffusivity may reflect the increase in axoplasmic flow in WM during the myelination period (Suzuki et al., 2003). Yet at the same time, axonal pruning may shorten the axon length and increase restriction (Bockhorst et al., 2008). The competition among these biological events makes it difficult to characterize the changes along axonal direction using conventional DTI. The trends of $\lambda_{//}$ in normal rodent brain development studies may easily become inconsistent due to these competing processes (Harsan et al., 2006; Larvaron et al., 2007). They would depend on different dominating biological factors, as well as the b -value and precise time point studied. In the present study, $K_{//}$ and $\lambda_{//}$ in WM were observed to increase concurrently. This finding indicated that DKI can yield more information regarding WM microstructure along the axonal direction.

At P13, the contrast between WM and GM in the kurtosis maps was not apparent (see Fig. 2). However, K_{\perp} difference between WM and GM increased substantially with age as shown in Figs. 2 and 3. It is known that there are premyelination modifications in WM that affect the diffusion properties, hence the FA in WM is higher in early postnatal stage (Huppi and Dubois, 2006; Neil et al., 2002). However, kurtosis measures did not detect these premyelination modifications as shown by their small differences between WM and GM at P13 (Figs. 2 and 3). Myelination in the rat brain begins at P10 (Bockhorst et al., 2008), which can increase K_{\perp} . In the present study, K_{\perp} in WM increased substantially after P13, especially in the highly restricted WM like CC or CP. This likely results from the myelination and dense packing of axon fibers, greatly enforcing the diffusion restriction in radial direction. In pathological cases, when there is myelin breakdown and debris formation, λ_{\perp} has been shown to increase while K_{\perp} decreases (Cheung et al., 2008; Hui et al., 2008).

It should be noted that kurtosis estimates can detect not only the WM changes but also GM. The complex maturation process in the relatively isotropic GM can be difficult to characterize by conventional DTI. However, kurtosis measurements in the present study revealed that the diffusion restriction in GM increases with ages (Fig. 3). This reflects the more densely packed structures like cells or membranes (Huppi and Dubois, 2006) and the dendritic architectural modifications in GM. It is also interesting to see most diffusivity changes in GM between P13 and P31 were significant while majority of the kurtosis changes between P31 and P120 were significant. More biological evidence is warranted to understand these specific observations. A trend of decreasing FA and increasing MK was observed in cortex (CT). This was likely a result of the transition of radial glia cells to astrocytes (Bockhorst et al., 2008; Chahboune et al., 2007; Sizonenko et al., 2007). As the main purpose of present study was to provide a general assessment of DKI, the cortical plate and cortical mantle were not measured separately as reported in other studies (Bockhorst et al., 2008; Sizonenko et al., 2007).

MK is shown here to be highly sensitive in detecting changes, but directional kurtoses are capable of providing more specific information on diffusion restriction along a particular direction (Cheung et al., 2008; Hui et al., 2008). For instance, more significant kurtosis changes in the radial direction of WM were observed as compared with those in axial direction in present study. While MK can serve as an indicator

to monitor normal brain maturation, the directional analysis can yield more sensitive detection of pathology that affects a particular direction. As K_{\perp} is highly sensitive to myelination, one would expect it capable of sensitively probing the demyelination processes in diseases such as multiple sclerosis.

Comparison between DKI and DTI derived diffusivities

The microstructural restriction in WM due to myelin sheath, axonal membrane or axonal packing increases with age, leading to more non-Gaussian diffusion and non-monoexponential b -value dependence. Therefore, approaches that are more accurate and sophisticated than conventional DTI are needed to extract extra information regarding such restricted diffusion environments. In Fig. 1, the signal attenuation is non-monoexponential. If a single non-zero b -value is used, for instance $b = 1 \text{ ms}/\mu\text{m}^2$ as in many conventional DTI studies, the signal attenuation cannot be fully characterized. The expanded logarithmic DKI quadratic model (Eq. (2)) enables us to describe the water diffusion behavior by both diffusivities and kurtoses. The combined use of these parameters ensures more sensitive characterization than fitting the signal decay to a monoexponential model. In the present study, DTI parameters obtained in DKI were compared to those derived by conventional DTI by fitting all DW signals of all b -values to monoexponential model for fair comparison of the two approaches. DW signals with a single non-zero b -value of $1 \text{ ms}/\mu\text{m}^2$ were also used to fit for diffusivities and comparisons among different age groups, yielding values and trends similar to those in Fig. 4 (not shown).

In fact, the diffusivity derived from conventional DTI manifests the combined and sometimes competing effects of the diffusivity and kurtosis derived in DKI. The relatively high sensitivity of the λ_{\perp} derived from monoexponential DTI model (shown in Fig. 4) was largely a result of increasing radial kurtosis with age while the radial diffusivity changes were moderate (Fig. 3). Therefore, the developmental changes in radial direction majorly act on diffusion restriction, hence radial kurtosis is expected to be more sensitive (K_{\perp} in Fig. 3 vs. λ_{\perp} in Fig. 4). DTI-derived $\lambda_{//}$ (in Fig. 4) is related to the increase of $K_{//}$ and $\lambda_{//}$ derived in DKI (in Fig. 3) that have opposite and competing effect. Thus its diminished sensitivity in detecting maturational changes (as shown by $\lambda_{//}$ in Fig. 4 vs. $K_{//}$ and $\lambda_{//}$ in Fig. 3) is expected. In other words, DKI-derived $K_{//}$ and $\lambda_{//}$ can greatly improve the level of significance and specificity in the analysis along axial direction. As the complex biological modification of WM along axonal direction affects both diffusivity and kurtosis, information obtained in conventional DTI is clearly inadequate to fully characterize the microstructural changes during brain maturation.

The present study again demonstrated that various diffusivity parameters estimated by conventional DTI, including FA, are b -value dependent. While applying different b -values may provide different physiological information (Jin and Kim, 2008), comparison among conventional DTI studies must be made with caution. The assumption of the monoexponential attenuation due to diffusion is invalid when the b -value is high, but high b -values can probe kurtosis information. The logarithmic quadratic DKI model demonstrated in present study allows the direct extraction of non-Gaussian or restricted diffusion information.

Conclusions

DKI has been demonstrated to be highly sensitive and directionally specific in detecting brain maturation processes. DKI approach quantifies both diffusivities and kurtoses; together they provided better detection and characterization of the developmental changes in various WM and GM structures studied. $K_{//}$ and K_{\perp} increased from P13 to P120, indicating generally more restricted diffusion environments. By measuring directional diffusivity and kurtosis, DKI offers a more

comprehensive and sensitive detection of subtle changes in tissue microstructure. Such imaging advance can provide better MR diffusion characterization of neural tissues, both WM and GM, in normal, developmental and pathological states.

Acknowledgments

We thank Dr. Jens H. Jensen at the New York University School of Medicine in New York and Dr. Hanzhang Lu at the UT Southwestern Medical Center in Dallas for assistance with data processing procedures. This work was supported in part by Hong Kong Research Grant Council and the University of Hong Kong Committee on Research and Conference Grants.

References

- Assaf, Y., Cohen, Y., 1998. Non-mono-exponential attenuation of water and N-acetyl aspartate signals due to diffusion in brain tissue. *J. Magn. Reson.* 131, 69–85.
- Assaf, Y., Mayk, A., Eliash, S., Speiser, Z., Cohen, Y., 2003. Hypertension and neuronal degeneration in excised rat spinal cord studied by high-*b* value *q*-space diffusion magnetic resonance imaging. *Exp. Neurol.* 184, 726–736.
- Assaf, Y., Chapman, J., Ben-Bashat, D., Hendler, T., Segev, Y., Korczyn, A.D., Graif, M., Cohen, Y., 2005. White matter changes in multiple sclerosis: correlation of *q*-space diffusion MRI and 1H MRS. *Magn. Reson. Imaging* 23, 703–710.
- Basser, P.J., 1995. Inferring microstructural features and the physiological state of tissues from diffusion-weighted images. *NMR Biomed.* 8, 333–344.
- Basser, P.J., Pierpaoli, C., 1996. Microstructural and physiological features of tissues elucidated by quantitative-diffusion-tensor MRI. *J. Magn. Reson. Ser. B* 111, 209–219.
- Basser, P.J., Jones, D.K., 2002. Diffusion-tensor MRI: theory, experimental design and data analysis – a technical review. *NMR Biomed.* 15, 456–467.
- Beaulieu, C., 2002. The basis of anisotropic water diffusion in the nervous system – a technical review. *NMR Biomed.* 15, 435–455.
- Beaulieu, C., Does, M.D., Snyder, R.E., Allen, P.S., 1996. Changes in water diffusion due to Wallerian degeneration in peripheral nerve. *Magn. Reson. Med.* 36, 627–631.
- Biton, I.E., Duncan, I.D., Cohen, Y., 2006. High *b*-value *q*-space diffusion MRI in myelin-deficient rat spinal cords. *Magn. Reson. Imaging* 24, 161–166.
- Bockhorst, K.H., Narayana, P.A., Liu, R., Ahobila-Vijjala, P., Ramu, J., Kamel, M., Wosik, J., Bockhorst, T., Hahn, K., Hasan, K.M., Perez-Polo, J.R., 2008. Early postnatal development of rat brain: in vivo diffusion tensor imaging. *J. Neurosci. Res.* 86, 1520–1528.
- Callaghan, P.T., 1991. Principles of Nuclear Magnetic Resonance Microscopy. Oxford University Press, Oxford England.
- Chahboune, H., Ment, L.R., Stewart, W.B., Ma, X., Rothman, D.L., Hyder, F., 2007. Neurodevelopment of C57BL/6 mouse brain assessed by in vivo diffusion tensor imaging. *NMR Biomed.* 20, 375–382.
- Cheung, M.M., Hui, E.S., Wu, E.X., 2008. Comparison of directional diffusion kurtoses and diffusivities in EAE-induced spinal cord. *Proc. Int. Soc. Magn. Reson. Med.* 16, 3328 (Toronto, Canada).
- Clark, C.A., Le Bihan, D., 2000. Water diffusion compartmentation and anisotropy at high *b* values in the human brain. *Magn. Reson. Med.* 44, 852–859.
- Clark, C.A., Hedehus, M., Moseley, M.E., 2002. In vivo mapping of the fast and slow diffusion tensors in human brain. *Magn. Reson. Med.* 47, 623–628.
- Dubois, J., Hertz-Pannier, L., Dehaene-Lambertz, G., Cointepas, Y., Le Bihan, D., 2006. Assessment of the early organization and maturation of infants' cerebral white matter fiber bundles: a feasibility study using quantitative diffusion tensor imaging and tractography. *Neuroimage* 30, 1121–1132.
- Falangola, M.F., Branch, C., Jensen, J.H., Hu, C., Xuan, L., Duff, K., Nixon, R., Helpert, J.A., 2007a. Assessment of brain microstructure in a transgenic mouse model of β -Amyloid deposition. *Proc. Int. Soc. Magn. Reson. Med.* 15, 310 (Berlin, Germany).
- Falangola, M.F., Ramani, A., Di Martino, A., Jensen, J.H., Babb, J.S., Hu, C., Szulc, K.U., Castellanos, F.X., Helpert, J.A., 2007b. Age-related patterns of change in brain microstructure by diffusional kurtosis imaging. *Proc. Int. Soc. Magn. Reson. Med.* 15, 667 (Berlin, Germany).
- Harsan, L.A., Poulet, P., Guignard, B., Steibel, J., Parizel, N., de Sousa, P.L., Boehm, N., Grucker, D., Ghandour, M.S., 2006. Brain dysmyelination and recovery assessment by noninvasive in vivo diffusion tensor magnetic resonance imaging. *J. Neurosci. Res.* 83, 392–402.
- Helpert, J.A., Falangola, M.F., Di Martino, A., Ramani, A., Babb, J.S., Hu, C., Jensen, J.H., Castellanos, F.X., 2007. Alterations in brain microstructure in ADHD by diffusional kurtosis imaging. *Proc. Int. Soc. Magn. Reson. Med.* 15, 1580 (Berlin, Germany).
- Hu, C., Jensen, J.H., Falangola, M.F., Helpert, J.A., 2008. CSF partial volume effect for diffusional kurtosis imaging. *Proc. Int. Soc. Magn. Reson. Med.* 16, 3325 (Toronto, Canada).
- Huang, H., Zhang, J., Wakana, S., Zhang, W., Ren, H., Richards, L.J., Yarowsky, P., Donohue, P., Graham, E., van Zijl, P.C., Mori, S., 2006. White and gray matter development in human fetal, newborn and pediatric brains. *Neuroimage* 33, 27–38.
- Hui, E.S., Cheung, M.M., Qi, L., Wu, E.X., 2008. Towards better MR characterization of neural tissues using directional diffusion kurtosis analysis. *Neuroimage* 42, 122–134.
- Huppi, P.S., Dubois, J., 2006. Diffusion tensor imaging of brain development. *Semin. Fetal Neonatal Med.* 11, 489–497.
- Jensen, J.H., Helpert, J.A., 2003. Quantifying non-Gaussian water diffusion by means of pulsed-field-gradient MRI. *Proc. Int. Soc. Magn. Reson. Med.* 11, 2154 (Toronto, Canada).
- Jensen, J.H., Helpert, J.A., Ramani, A., Lu, H., Kaczynski, K., 2005. Diffusional kurtosis imaging: the quantification of non-Gaussian water diffusion by means of magnetic resonance imaging. *Magn. Reson. Med.* 53, 1432–1440.
- Jin, T., Kim, S.G., 2008. Functional changes of apparent diffusion coefficient during visual stimulation investigated by diffusion-weighted gradient-echo fMRI. *Neuroimage* 41, 801–812.
- Jones, D.K., Horsfield, M.A., Simmons, A., 1999. Optimal strategies for measuring diffusion in anisotropic systems by magnetic resonance imaging. *Magn. Reson. Med.* 42, 515–525.
- Larvaron, P., Boespflug-Tanguy, O., Renou, J.P., Bonny, J.M., 2007. In vivo analysis of the post-natal development of normal mouse brain by DTI. *NMR Biomed.* 20, 413–421.
- Latt, J., Nilsson, M., Wirestam, R., Johansson, E., Larsson, E.M., Stahlberg, F., Brockstedt, S., 2008. In vivo visualization of displacement-distribution-derived parameters in *q*-space imaging. *Magn. Reson. Imaging* 26, 77–87.
- Liu, C., Bammer, R., Acar, B., Moseley, M.E., 2004. Characterizing non-Gaussian diffusion by using generalized diffusion tensors. *Magn. Reson. Med.* 51, 924–937.
- Lu, H., Jensen, J.H., Ramani, A., Helpert, J.A., 2006. Three-dimensional characterization of non-Gaussian water diffusion in humans using diffusion kurtosis imaging. *NMR Biomed.* 19, 236–247.
- Minati, L., Aquino, D., Rampoldi, S., Papa, S., Grisoli, M., Bruzzone, M.G., Maccagnano, E., 2007. Biexponential and diffusional kurtosis imaging, and generalised diffusion-tensor imaging (GDTI) with rank-4 tensors: a study in a group of healthy subjects. *Magma* 20, 241–253.
- Mori, S., Itoh, R., Zhang, J., Kaufmann, W.E., van Zijl, P.C., Solaiyappan, M., Yarowsky, P., 2001. Diffusion tensor imaging of the developing mouse brain. *Magn. Reson. Med.* 46, 18–23.
- Moseley, M.E., Cohen, Y., Kucharczyk, J., Mintorovitch, J., Asgari, H.S., Wendland, M.F., Tsuruda, J., Norman, D., 1990. Diffusion-weighted MR imaging of anisotropic water diffusion in cat central nervous system. *Radiology* 176, 439–445.
- Mulkern, R.V., Gudbjartsson, H., Westin, C.F., Zengingonul, H.P., Gartner, W., Guttman, C.R., Robertson, R.L., Kyriakos, W., Schwartz, R., Holtzman, D., Jolesz, F.A., Maier, S.E., 1999. Multi-component apparent diffusion coefficients in human brain. *NMR Biomed.* 12, 51–62.
- Neil, J., Miller, J., Mukherjee, P., Huppi, P.S., 2002. Diffusion tensor imaging of normal and injured developing human brain – a technical review. *NMR Biomed.* 15, 543–552.
- Niendorf, T., Dijkhuizen, R.M., Norris, D.G., van Lookeren Campagne, M., Nicolay, K., 1996. Biexponential diffusion attenuation in various states of brain tissue: implications for diffusion-weighted imaging. *Magn. Reson. Med.* 36, 847–857.
- Nossin-Manor, R., Duvdevani, R., Cohen, Y., 2007. Spatial and temporal damage evolution after hemi-crush injury in rat spinal cord obtained by high *b*-value *q*-space diffusion magnetic resonance imaging. *J. Neurotrauma* 24, 481–491.
- Paxinos, G., Watson, C., 2005. The Rat Brain in Stereotaxic Coordinates – the New Coronal Set, 5th edition ed. Elsevier Academic Press, San Diego.
- Ozarslan, E., Mareci, T.H., 2003. Generalized diffusion tensor imaging and analytical relationships between diffusion tensor imaging and high angular resolution diffusion imaging. *Magn. Reson. Med.* 50, 955–965.
- Qi, L., Wang, Y., Wu, E.X., 2008. D-eigenvalues of diffusion kurtosis tensors. *J. Comput. Appl. Math.* 221, 150–157.
- Ramani, A., Jensen, J.H., Szulc, K.U., Ali, O., Hu, C., Lu, H., Brodte, J.D., Helpert, J.A., 2007. Assessment of abnormalities in the cerebral microstructure of schizophrenia patients: a diffusional kurtosis imaging study. *Proc. Int. Soc. Magn. Reson. Med.* 15, 648 (Berlin, Germany).
- Sizonenko, S.V., Camm, E.J., Garbow, J.R., Maier, S.E., Inder, T.E., Williams, C.E., Neil, J.J., Huppi, P.S., 2007. Developmental changes and injury induced disruption of the radial organization of the cortex in the immature rat brain revealed by in vivo diffusion tensor MRI. *Cereb. Cortex* 17, 2609–2617.
- Song, S.K., Sun, S.W., Ju, W.K., Lin, S.J., Cross, A.H., Neufeld, A.H., 2003. Diffusion tensor imaging detects and differentiates axon and myelin degeneration in mouse optic nerve after retinal ischemia. *Neuroimage* 20, 1714–1722.
- Sun, S.W., Neil, J.J., Liang, H.F., He, Y.Y., Schmidt, R.E., Hsu, C.Y., Song, S.K., 2005. Formalin fixation alters water diffusion coefficient magnitude but not anisotropy in infarcted brain. *Magn. Reson. Med.* 53, 1447–1451.
- Sun, S.W., Liang, H.F., Le, T.Q., Armstrong, R.C., Cross, A.H., Song, S.K., 2006. Differential sensitivity of in vivo and ex vivo diffusion tensor imaging to evolving optic nerve injury in mice with retinal ischemia. *Neuroimage* 32, 1195–1204.
- Suzuki, Y., Matsuzawa, H., Kwee, I.L., Nakada, T., 2003. Absolute eigenvalue diffusion tensor analysis for human brain maturation. *NMR Biomed.* 16, 257–260.
- Tuch, D.S., Reese, T.G., Wiegell, M.R., Makris, N., Belliveau, J.W., Wedeen, V.J., 2002. High angular resolution diffusion imaging reveals intravoxel white matter fiber heterogeneity. *Magn. Reson. Med.* 48, 577–582.
- Verma, R., Mori, S., Shen, D., Yarowsky, P., Zhang, J., Davatzikos, C., 2005. Spatiotemporal maturation patterns of murine brain quantified by diffusion tensor MRI and deformation-based morphometry. *Proc. Natl. Acad. Sci. U S A* 102, 6978–6983.
- Wang, Y., Cheung, P.T., Shen, G.X., Wu, E.X., Cao, G., Bart, I., Wong, W.H., Khong, P.L., 2006. Hypoxic-ischemic brain injury in the neonatal rat model: relationship between lesion size at early MR imaging and irreversible infarction. *AJNR Am. J. Neuroradiol.* 27, 51–54.
- Wang, S., Wu, E.X., Tam, C.N., Lau, H.F., Cheung, P.T., Khong, P.L., 2008. Characterization of white matter injury in a hypoxic-ischemic neonatal rat model by diffusion tensor MRI. *Stroke* 39, 2348–2353.
- Woods, R.P., Grafton, S.T., Holmes, C.J., Cherry, S.R., Mazziotta, J.C., 1998. Automated image registration: I. General methods and intrasubject, intramodality validation. *J. Comput. Assist. Tomogr.* 22, 139–152.
- Yang, J., Wu, E.X., 2008. Detection of cortical gray matter lesion in the late phase of mild hypoxic-ischemic injury by manganese-enhanced MRI. *Neuroimage* 39, 669–679.
- Yang, J., Khong, P.L., Wang, Y., Chu, A.C., Ho, S.L., Cheung, P.T., Wu, E.X., 2008. Manganese-enhanced MRI detection of neurodegeneration in neonatal hypoxic-ischemic cerebral injury. *Magn. Reson. Med.* 59, 1329–1339.
- Zhang, J., Richards, L.J., Yarowsky, P., Huang, H., van Zijl, P.C., Mori, S., 2003. Three-dimensional anatomical characterization of the developing mouse brain by diffusion tensor microimaging. *Neuroimage* 20, 1639–1648.